Sustainable Energy & Fuels

# The Oxygen Reduction Reaction Catalyzed by *Synechocystis* sp. PCC 6803 Flavodiiron Proteins



| | |
|---|---|
| Journal: | *Sustainable Energy & Fuels* |
| Manuscript ID | SE-ART-07-2019-000523.R1 |
| Article Type: | Paper |
| Date Submitted by the Author: | 10-Sep-2019 |





| | |
|---|---|
| Complete List of Authors: | Brown, Katherine; National Renewable Energy Laboratory, Biosciences Center; National Renewable Energy Lab<br>Guo, Zhanjun; National Renewable Energy Laboratory,<br>Tokmina-Lukaszewska , Monika; Montana State University Bozeman, Department of Chemistry and Biochemistry<br>Scott, Liam; Montana State University Bozeman, Department of Chemistry and Biochemistry<br>Lubner, Carolyn ; National Renewable Energy Laboratory<br>Smolinski, Sharon; National Renewable Energy Laboratory, Biosciences Center<br>Mulder, David; National Renewable Energy laboratory,<br>Bothner, Brian; Montana State University Bozeman, Department of Chemistry and Biochemistry<br>King, Paul; National Renewable Energy Laboratory, |

ARTICLE

# The Oxygen Reduction Reaction Catalyzed by *Synechocystis* sp. PCC 6803 Flavodiiron Proteins

Received 00th January 20xx,
Accepted 00th January 20xx

DOI: 10.1039/x0xx00000x

Katherine A. Brown[a], Zhanjun Guo[a], Monika Tokmina-Lukaszewska[b], Liam W. Scott[b], Carolyn E. Lubner[a], Sharon Smolinski[a], David W. Mulder[a], Brian Bothner[a], and Paul W. King[b*]

Photosynthetic flavodiiron (Flv) proteins bind flavin and non-heme Fe cofactors and catalyze the oxygen reduction reaction (ORR) coupled to oxidation of reduced pyridine nucleotides during photosynthetic growth. The activity of Flvs have also been observed to form an important catalytic redox loop with water oxidation necessary for preserving photosynthetic electron transport function in cynaobacteria. To determine how these functions may be related we investigated the kinetic properties of Flv1 and Flv3 from Synechocystis sp. PCC 6803. Under an oxygen atmosphere, Flv1 and Flv3 were found to catalyze ORR with either NADH or NADPH as the electron donor. Reaction velocity curves were sigmoidal and Flv binding of NAD(P)H was cooperative. Based on mass spectrometry generated structural models, each Flv assembles as a homodimer with two oxidoreductase domains capable of binding two molecules of NAD(P)H per subunit, and flavins arranged to support electron transfer to the diiron sites for oxygen reduction. Titrations with NAD(P)H resulted in reduction of the diiron site without the accumulation of stable, reduced flavin intermediates. Altogether, the results provide new insights on the properties of Flv1 and Flv3 that enable tight control of rectivity for the complete reduction of oxygen to water, and in this capacity help preserve photosynthetic electron transport function.

## Introduction

Flavodiiron proteins (FDPs) comprise a large family of enzymes that catalyze the oxygen ($O_2$) reduction reaction (ORR) or nitric oxide (NO) reduction reaction (NOR).[1] In photosynthetic microbes like *Synechocystis*, ORR forms a redox loop with the light-driven $O_2$ evolution reaction catalyzed by Photosystem II.[2, 3] The electrochemical steps that couple the two half-reactions generate proton motive force used to catalyze ATP formation.[4] ORR catalysts are also fundamental components of fuel cell devices that couple $O_2$ reduction to the oxidation of a chemical fuel (e.g., hydrogen) generating an electrical current to power devices. For these applications, there remain significant challenges to developing ORR catalysts that are selective, efficient, economical and able to operate at the high rates required for practical devices.[5, 6] As a result, studies on the mechanisms of $O_2$ activating enzymes may provide important insights on how to overcome limitations faced by current ORR catalyst designs.

The structural composition of FDPs share a common two-domain framework consisting of a non-heme diiron binding domain for $O_2$/NO activation and an electron relay flavodoxin-like domain, with subclasses that incorporate additional domains.[7] Structures of two-domain FDPs are organized as homodimers of identical subunits where the flavin of one subunit is adjacent to the diiron site of the other subunit. During catalysis, reductant transfer to FDPs by a cognate NAD(P)H oxidoreductase enzyme leads to reduction of the flavin cofactor followed by electron transfer to the adjacent diiron center.[8-10] Thus, the homodimer structure of FDPs organizes the cofactors to enable inter-subunit electron transfer during catalytic turnover.[11]

Compared to standard two-domain FDPs, the FDPs from oxygenic photosynthetic organisms (referred to here as Flvs) differ by incorporating an NAD(P)H oxidoreductase domain with an additional flavin binding site. This additional domain was demonstrated in recombinant cyanobacterial Flv3 to enable NAD(P)H-dependent $O_2$ uptake, with turnover frequencies (TOF) were 0.2-0.4 $min^{-1}$ with a $K_m$ for NADH of 22.4 μM and NADPH of 130 μM.[3] Moreover, a Flv4-GST fusion also catalyzed NADH-dependent $O_2$ uptake, although at a 10-fold higher TOF of 20 $min^{-1}$, with a preference for NADH ($K_m$ = 30 μM) and a reported $K_m$ of 10 μM for $O_2$.[12] Recently, an X-ray structure of a subunit of Flv1 from *Synechocystis* sp. PCC 6803 (*S.* 6803) lacking the oxidoreductase domain was solved.[13] Although the Flv1 partial structure presents new details on the properties of Flvs, it leaves open the question of how the oxidoreductase domain is oriented to couple NAD(P)H oxidation with electron flow to the diiron sites, nor did it provide definitive evidence on the identity of the flavin cofactors. In addition, the outcome of the studies did not completely address a proposed function of

[a] National Renewable Energy Laboratory, Golden, Colorado, USA. Email: paul.king@nrel.gov
[b] Department of Chemistry and Biochemistry, Montana State University, Bozeman, Montana USA.
†Electronic Supplementary Information (ESI) available: See DOI: 10.1039/x0xx00000x

Flvs in photosynthetic electron flow and protection of photosynthetic reaction centers from $O_2$ damage.

To address the knowledge gaps in Flvs and provide more details on the NAD(P)H and $O_2$ reactivity, ORR kinetics, and structures, we conducted studies on *S.* 6803 Flv1 and Flv3. These two Flvs are involved in alternative electron flow in photosynthetic In order to decipher the kinetic properties unique to photosynthetic Flvs, StrepII-tagged *S.* 6803 Flv1 and Flv3 were recombinantly produced in *Escherichia coli*, and affinity purified to homogeneity (Figure S1). The molecular weights on SDS-PAGE were ~ 66 and 65 kDa for Flv1 and Flv3, respectively. Due to incomplete incorporation of Fe and flavin based on cofactor analysis, the two enzymes were reconstituted with an excess of Fe and flavin, which resulted in a stoichiometric ratio of 2 flavins and 2 Fe atoms per-subunit (Tables S1 and S2).

## Results and discussion

### *S.* 6803 Flv1 and Flv3 catalyze the $O_2$ reduction reaction coupled to oxidation of NAD(P)H

Both of the reconstituted Flvs catalyzed oxidation of NAD(P)H under atmospheric (223 µM) levels of $O_2$ with $k_{cat}$ values of 47 and 26 $s^{-1}$ (NADH) and 25 and 32 $s^{-1}$ (NADPH) by Flv1 and Flv3, respectively (Table S3). Plots of the reaction rate dependence on NAD(P)H (Figure S2, Table S4) were best fit by a sigmoidal (Hill) versus hyperbolic (Michaelis-Menten) function (Table S5). Fits to the Hill equation (Eqn 1) gave a Hill coefficient of ~2 for NAD(P)H and *K'* values (analogous to the $K_m$ from a Michaelis-Menten kinetic fit) of ~100 µM (Table 1) showing these two Flvs have near equal affinity for NADH and NADPH.

Table 1. Hill kinetics of ORR for Flv1 and Flv3.

| Flv | NAD(P)H | $K'$ [a] | $V_{max}$ [b] | $k_{cat}$ ($s^{-1}$) | $n$[b] | $k_{cat}/K'$ ($M^{-1}$ $s^{-1}$)[c] |
|---|---|---|---|---|---|---|
| 1 | NADH | 184 ± 29 | 37 ± 3 | 40 | 2.1 ± 0.6 | 2.2 x $10^5$ |
| | NADPH | 152 ± 28 | 28 ± 2 | 30 | 2.4 ± 0.5 | 2.0 x $10^5$ |
| 3 | NADH | 256 ± 29 | 33 ± 3 | 35 | 1.8 ± 0.5 | 1.4 x $10^5$ |
| | NADPH | 201 ± 18 | 28 ± 2 | 30 | 2.3 ± 0.4 | 1.5 x $10^5$ |

[a]Values of $K'$ (µM $O_2$) were obtained from fits to the steady-state Hill equation (Eqn 1) in reactions with 1 mM NAD(P)H (± SEM). Individual rate values are shown in Table S6.

[b]µmol $O_2$ $mg^{-1}$ $min^{-1}$ (± SEM). Hill coefficient (n) for $O_2$ (± SEM).

[c]per-subunit.

The Flv1 and Flv3 ORR dependence on $O_2$ was also best fit to a Hill function (Figure 1, Table S7), with Hill coefficients of ~2 and $K'$ values for $O_2$ near 200 µM (Table 1). This value is significantly higher than the ~2-7 µM $K_m$ values previously reported for FDPs[14, 15] and closely matches the steady-state $O_2$ concentrations of *S.* 6803 during photosynthetic growth.[16] The $k_{cat}$ values were 30-40 $s^{-1}$ with 223 µM $O_2$ (Table 1) and 60-80 $s^{-1}$ under saturating $O_2$ (1066 µM, 100% $O_2$ atmosphere, Table S8). The efficiencies for ORR catalysis of both Flvs were 105 $M^{-1}$ $s^{-1}$ with either NADH or NADPH. This stands in contrast to FDPs that preferentially use NADH for ORR catalysis and exhibit microbes, and proposed to function in protection of Photosystem I (PSI) from $O_2$ induced damage. These results are discussed in the context of how the ORR kinetic properties of Flv1 and Flv3 are specifically adapted to suit their function as components of the alternative redox pathways coupled to photosynthetic electron flow.

Michaelis-Menten kinetics.[15, 17, 18] Under optimal reaction conditions the ratio of $V_{max}$ values of Flv1 and Flv3 for NAD(P)H oxidation to ORR are ~2:1 (Table S8) indicating the reduction of two molecules of $O_2$ proceeds by a four electron reduction process.

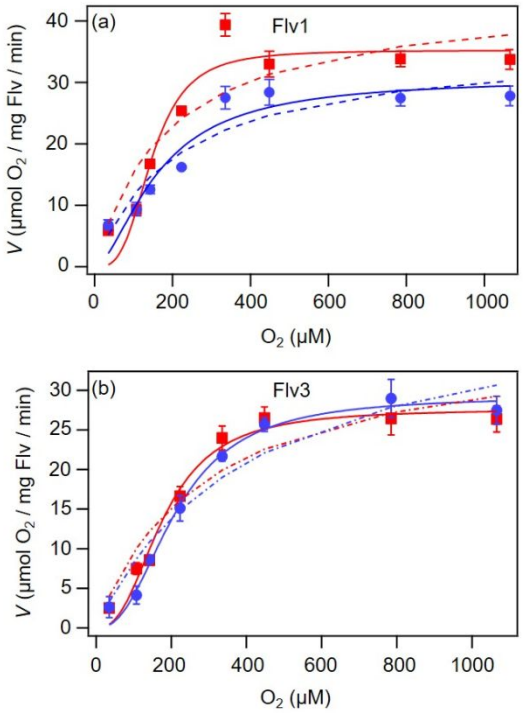


**Figure 1**. The $O_2$ concentration dependence of Flv1 and Flv3 ORR kinetics. (a) Flv1 ORR with NADH (red squares) or NADPH (blue circles). (b) Flv3 ORR with NADH (red squares) or NADPH (blue circles). Solid lines are fits to the steady-state Hill equation (Eqn 1). Dashed lines are fits to the steady-state Michaelis-Menten equation (Eqn 2). Reactions were performed with 12.5 nM Flv and 1 mM of either NADH or NADPH in 50 mM MOPS, pH 7, 5% glycerol. Plots are averages of N=2 reactions. Values for each plot are shown in Table S6.

The catalytic efficiencies of Flv1 and Flv3 for ORR in Table 1 are ~$10^3$-$10^4$ fold higher than NAD(P)H-dependent ORR kinetics previously reported for Flv3 ($k_{cat}/K_m$ = ~44 $M^{-1}$ $s^{-1}$ for NADH and 8 $M^{-1}$ $s^{-1}$ for NADPH),[3] and 10-fold higher than the value reported for NADH-dependent ORR by Flv4-GST ($k_{cat}/K_m$ = $10^4$ for $O_2$ and NADH).[12] The higher efficiencies reported here may reflect differences in enzyme quality compared to previous preparations,[3, 12] for example, lower stoichiometric cofactor incorporation of either Fe or flavin, or lower enzyme stability.

### NAD(P)H binding by Flv1 and Flv3 is cooperative

The fact that Flvs contain an oxidoreductase domain and require 2 NAD(P)H per-$O_2$ in the reaction cycle led us to hypothesize that the cooperative kinetics of Flvs may result from cooperative binding of NAD(P)H by Flv. To test this, we

performed titrations of Flv1 and Flv3 with NAD(P)H and monitored quenching of the intrinsic Trp and Tyr fluorescence emission at 348 nm. As shown in Figure 2, quenching of the Flv 348 nm fluorescence coincided with the appearance of an NAD(P)H emission peak at 457 nm signifying fluorescence resonance energy transfer (FRET) between Trp or Tyr and Flv-bound NAD(P)H.[19, 20] The NAD(P)H equilibrium binding isotherms (determined from Eqns. 2-6 and plotted in Figure 2) were best fit to the Hill equation (Eqn 1) with μM $K_d$ values (Table 2) that are similar in magnitude to the $K'$ values determined for NAD(P)H-dependent ORR. Overall, fits of Flv fluorescence changes with changing [NAD(P)H] indicate a positive homotropic response, demonstrating that binding of NAD(P)H to one subunit increases the affinity for NAD(P)H by the other subunit.[21, 22]

Table 2. Flv1 and Flv3 NAD(P)H binding kinetics.

| Flv | NADH | | NADPH | |
|---|---|---|---|---|
| | $K_d$[a] | $n$[b] | $K_d$[a] | $n$[b] |
| 1 | 305 ± 61 | 1.6 ± 0.6 | 175 ± 34 | 1.8 ± 0.5 |
| 3 | 304 ± 25 | 1.9 ± 0.2 | 219 ± 46 | 1.8 ± 0.4 |

[a]Fits to Eqns 3-7, values in μM (± SEM).

[b]Hill coefficient fits to Eqn 7 (± SEM).

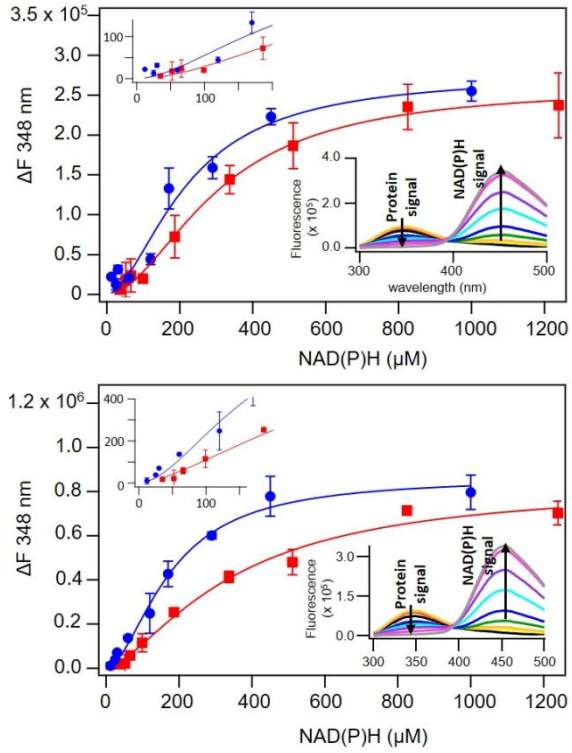


**Figure 2**. NAD(P)H equilibrium binding isotherms for Flv1 and Flv3. (top) Flv3, (bottom) Flv1 binding isotherm with either NADH (red squares) or NADPH (blue circles). Solid lines are fits to Eqn 5. Upper insets, magnification of the initial isotherm values to show the sigmoidal dependence of Δ$F$ on [NAD(P)H]. Lower insets, Flv fluorescence emission spectra decreases with increasing [NAD(P)H]. [NAD(P)H] = 0 μM, black; 35 μM, red; 50 μM, orange; 65 μM, yellow; 100 μM, green; 185 μM, blue; 335 μM, light blue; 500 μM, purple; 825 μM, pink; and 1250 μM, grey. All reactions were performed anaerobically with 200 nM Flv in 50 mM MOPS, pH 7, 5% glycerol. $\Delta F = F_{NAD(P)H} - F_0$, where $F_{NAD(P)H}$ is the fluorescence signal at 348 nm at a given [NAD(P)H] and $F_0$ is the fluorescence signal at 348 nm for Flv alone. Excitation wavelength, 285 nm, emission scan 300 - 500 nm with slits at 8 nm.

**Flv3 assembles as homodimers**

In order to address whether the structures of Flvs can enable cooperative kinetics we analyzed Flv3, which we could produce at higher amounts, for Mass Spectrometry (MS). To define the oligomeric states and cofactor compositions of Flv3 we used chemical cross-linking (Figure 3a-c). Liquid Chromatography MS (LCMS) analysis of the cross-linked Flv3 identified a higher molecular weight population consistent with homodimers (Figure 3a). Since Flv3 was reconstituted in the presence of both FMN and FAD, reverse phase (RP) LCMS was used to determine the identity of the flavin content. The RP-LCMS process denatures the Flv3 homodimer to permit separation of the protein and cofactors. As shown in Figure 3b, the extracted ion current of the flavin fraction revealed only the presence of FMN (purple trace).

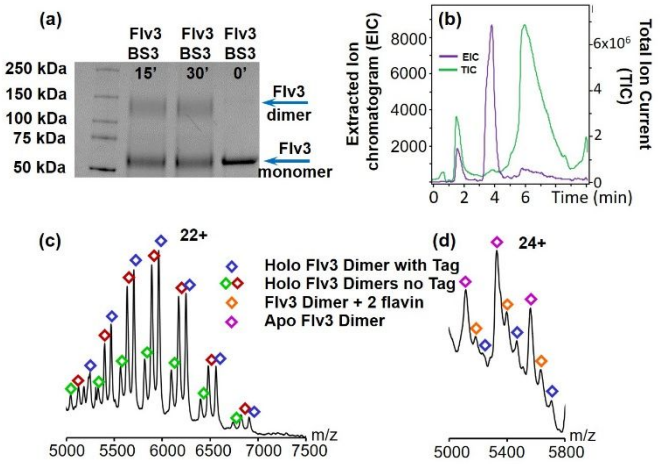


**Figure 3**. Oligomeric state and cofactor composition of Flv3. (a) SDS-PAGE of Flv3 subunit (65 kD) and homodimer (130 kD) in solution after cross-linking with 1 mM bis(sulfosuccinimidyl)suberate (BS3). Only Flv3 peptides were detected by LC-MS/MS. (b) Reverse phase separation of Flv3 homodimers. The denatured Flv3 subunit component, without the FMN cofactor, is in green (total ion current, TIC). The extracted flavin cofactor component is in purple (extracted ion chromatogram, EIC), which confirmed the presence of FMN. (c) Native mass spectrum of Flv3 holo-homodimers. Charge state distributions of Flv3 samples show dimers with (blue) and without (red and green) Strep-II affinity tag. (d) Native mass spectrum of partially dissociated Flv3 homodimer reveals three species: a cofactor replete (holo), cofactor deplete (apo), and partially dissociated intermediate (homodimer + 2 flavins).

Native MS of Flv3 was performed under mild collisional activation, which identified three distinct species (Figures 3c and 3d). One was the fully enriched holo-homodimer (with four flavins, and four Fe atoms). Another was a partially dissociated intermediate homodimer (two flavins), and a third fraction was composed of apo-homodimers. The native MS and cross-linked LCMS results show that flavin binding by Flv3 homodimers is partially labile, with a preference for FMN. In support of this conclusion, a separate phosphodiesterase digestion[23] of the reconstituted Flv3 gave a 1:3 FAD:FMN ratio (Table S2), consistent with previous reports.[3] We hypothesize that the formation of partially replete homodimers and absence of FAD in the LCMS analysis might be due to the loss of a more labile FMN/FAD cofactor during the spin filtration treatment.

**Defining the reduction-oxidation state of Flv3 in reactions with NAD(P)H and $O_2$**

To understand the process by which Flvs couple NAD(P)H oxidation to $O_2$ reduction we studied changes in Flv3 reduction-oxidation state using a combination of UV-Vis and EPR spectroscopy (Figures S3, 4 and 5, respectively). The UV-Vis and EPR spectra of the as-purified, aerobic Flv3 in Figure S3 and Figure 5, respectively, show characteristic oxidized flavin peaks at 380 nm and 454 nm accompanied by a weak EPR signal at *g* = 2.00 reflective of an organic type radical and the absence of a paramagnetic Fe signal. This spectrum presumably represents the fully oxidized flavin and diamagnetic $Fe^{3+}Fe^{3+}$ oxidation state of Flv3.

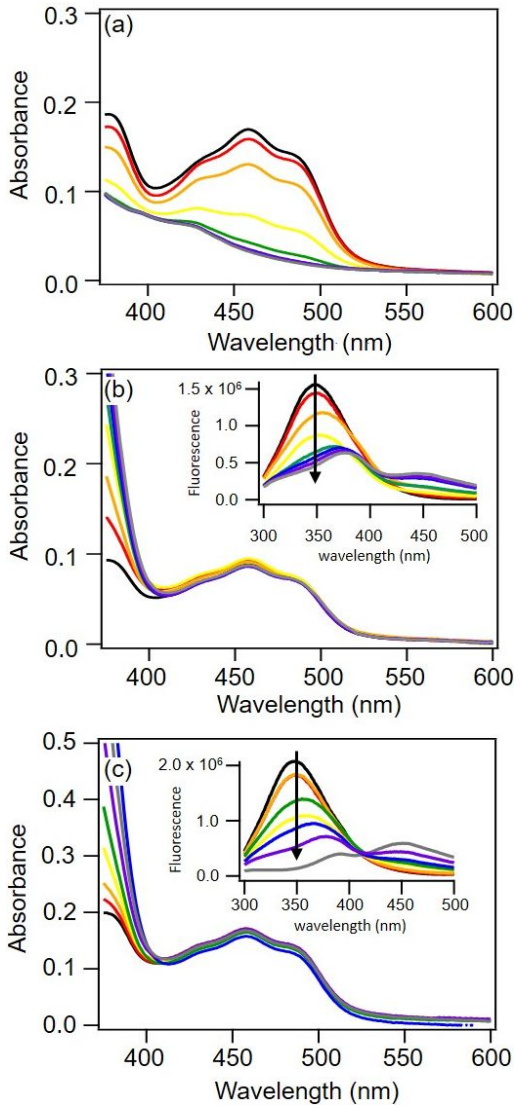


**Figure 4.** UV-Visible spectroscopy of Flv3 under anaerobic reduction. (a) Titration with sodium dithionite. (b) Titration with NADPH. (c) Titration with NADH. Insets of (b) and (c) are the Flv3 tryptophan fluorescence signal with increasing molar ratios of NAD(P)H, arrow indicates the decrease in fluorescence with increased amounts of NAD(P)H. Plots show molar ratios of reductant:Flv3 at 0:1 (black), 2:1 (red), 4:1 (orange), 6:1 (yellow), 8:1 (green), 10:1 (blue), 12:1 (purple), and 14:1 (grey). All reactions were performed with 25 µM Flv3 in 50 mM MOPS, pH 7, 5% glycerol.

The UV-Vis spectra of anaerobic Flv3 titratrd with sodium dithionite showed bleaching of the oxidized flavin and complete 2-electron reduction to the hydroquinone state (Figure 4a). A peak characteristic of a 1-electron reduced semiquinone (SQ), typically observed at either 390 nm or 600 nm, was not evident in the reduced Flv3 spectrum. The lack of an observable SQ in Flvs is similar to what has been reported for reduced FDPs, suggesting that electron transfer by the flavin is likely to involve a kinetically destabilized, short-lived semiquinone.[18] The corresponding EPR spectrum of Flv3 treated with an excess of sodium dithionite under anaerobic conditions resulted in a silent spectrum (Figure 5, green trace), indicative of reduction of both the radical species and diiron site to the diamagnetic $Fe^{2+}Fe^{2+}$ oxidation state.

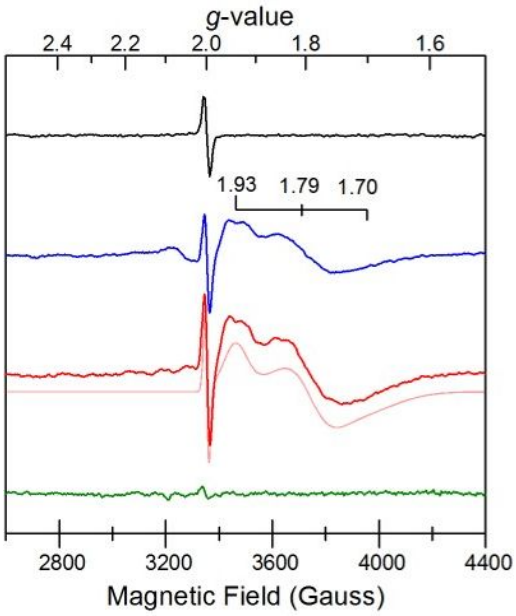


**Figure 5**. EPR spectra of oxidized and reduced Flv3. Black trace (top), as-isolated, air-oxidized sample. Blue trace (second from top), anaerobic sample reduced with NADPH. Red trace (third from top), anaerobic sample reduced with NADH (light red, composite simulation of radical and diiron, mixed valent $Fe^{3+}Fe^{2+}$ signals). Green trace (bottom), anaerobic sample reduced with sodium dithionite. Microwave frequency, 9.38 GHz; microwave power, 1 mW; sample temperature, 5K. Flv3 was at 100 µM.

Under anaerobic titration with NAD(P)H, the UV-Vis spectra of Flv3 indicated the binding of NAD(P)H based on quenching of the intrinsic protein fluorescence signal (Figures 4b and 4c), without formation of a reduced flavin that was observed under reduction with sodium dithionite. The EPR spectrum of Flv3 treated with NADH or NADPH produced a rhombic type signal that could be simulated with *g*-values at 1.93, 1.79, 1.70, and assigned to a $S = ½$ state antiferromagnetically coupled $Fe^{3+}Fe^{2+}$ site. Similar signals with $g_{avg} < 2$ have been observed in other FDPs[17, 18, 24, 25] and non-heme diiron proteins and is considered the canonical fingerprint for the mixed-valent diiron site.[26, 27] Here, the diiron signal was most intense at 5 K, significantly broadened at 15 K, and could not be detected above 25 K. In addition, a radical signal at $g = 2.00$, slightly increased in intensity and displayed similar temperature dependency (data not shown) to the diiron signal, also becoming undetectable above 35 K. Both signals displayed similar power saturation behavior (diiron $P_{½} = 8.7$ mW, radical $P_{½} = 3.6$ mW at 5 K), with the diiron signal saturating slightly more strongly at higher

powers (Figure S4). The combined UV-Vis and EPR results indicate the absence of a stable reduced flavin intermediate, although the nature of the radical signal observed in EPR and its paramagnetic properties do not allow for a definitive assignment. The absence of a long-lived reduced flavin state during NAD(P)H oxidation suggests a rapid coupling to the two-electron reduction of the diiron site. Moreover, binding and oxidization of multiple molecules of NAD(P)H is unlikely based on a lack of accumulation of reduced species (i.e., only the radical and reduced $Fe^{3+}Fe^{2+}$ diiron site were observed).

**Flv structures form intramolecular electron transfer pathways**

To understand how the unique properties of Flvs are enabled by the incorporation of the oxidoreductase domain in a homodimer structure that supports cooperative binding of NAD(P)H and coupling of NAD(P)H oxidation to electron transfer and $O_2$ reduction by the diiron site, we used MS to develop 3D models of the quaternary structure of Flv3. We first mapped the solvent accessible surface of intact Flv3 homodimers by two surface-labelling reagents, glycine ethyl ester (GEE) and dansyl chloride (DnsCl) that have orthogonal chemistry and target the most prevalent groups on protein surfaces (carboxyl, primary amine, and hydroxyl groups). The results from time course labelling experiments are summarized in Figures S5 and S6. Reagent labelling of the oxidoreductase domain was observed at the exposed surface or the NAD(P)H binding site, but not inside the binding cavity (Figures 6a, 6b, and S6a). A large inaccessible region was identified that we propose forms the dimer interface. Reactions with DnsCl and GEE also indicated that the predicted FMN binding site in the flavodoxin-like domain and the diiron binding pocket are not solvent accessible, since labelling was observed near, but not at, the predicted FMN and diiron sites despite the presence of available residues. This suggests that the binding surface of Flv3 subunits must encompass the FMN and diiron binding sites. This is possible when two subunits are arranged in a "head-to-tail" orientation within a complex.

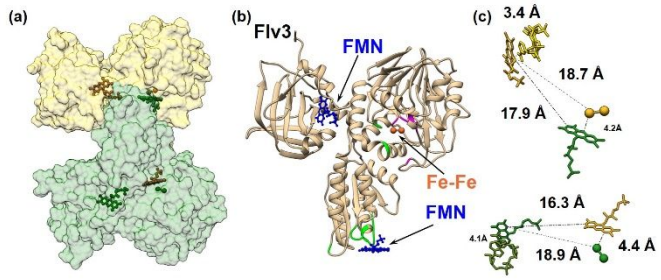


**Figure 6**. Homology models of Flv3. (a) Flv3 homodimer selected from 28 similar ClusPro generated homodimer configurations based on acceptable distance constraints (less than 10 Å) between diiron, FMN cofactors and complete agreement with surface labelling results. (b) Flv3 subunit showing the location of FMN and diiron cofactor sites. The Flv3 residues having direct interactions with FMN (green) and diiron (magenta) based on predicted Flv3 structure are highlighted. A second flavin was added to the Flv3 oxidoreductase domains based on homology to HpaC using the Chimera match maker function [28] (c) Model of an electron flow pathway between cofactor sites in a Flv3 homodimer. Dotted lines indicate calculated inter-cofactor distances.

Analysis of the cofactor-to-cofactor distances in the homodimer model in Figure 6c indicates that they are reasonable to support electron transfer from NAD(P)H oxidation at the oxidoreductase domain to the reduction of the diiron site (additional distances in Table S9 and Figure S7). There are also approximately 11 Trp and Tyr residues that surround the diiron site within a radius of ~25 Å. One or more of these residues may account for the organic radical signal observed by EPR in NAD(P)H-reduced Flv3 (Figure 5). Trp and Tyr radicals have been implicated in the mechanisms of some FDPs as well as other mono- or diiron proteins like ribonucleotide reductase.[29-31] Chains of Trp and Tyr residues have also been proposed to form "radical escapes routes" for prevention of radical induced damage.[30, 31]

## Conclusions

The studies reported here on Flv1 and Flv3 extend on the initial ORR kinetics of Flvs and partial X-ray structure of Flv1[3, 12, 13] and provide more insights into the Flv structure, substrate reactivity and ORR catalysis. The measured catalytic efficiencies of $10^5$ $M^{-1}$ $s^{-1}$ are similar to the values reported for other $O_2$-reducing FDPs,[32] and fall within the range of $10^2$-$10^6$ $M^{-1}$ $s^{-1}$ for homogeneous molecular catalysts for which water is the major ORR product.[6] The binding reactivities for $O_2$ and NAD(P)H are consistent with Flvs functioning under the $O_2$-rich physiologies of photosynthetic microbes with NAD(P)H levels that range from 100-130 µM for NADH and 480-650 µM NAD(P)H.[33] A catalytic efficiency of $10^5$ $M^{-1}$ $s^{-1}$ for ORR by Flv1 and Flv3 is higher than that of the Mehler reaction of ferredoxin reduction of $O_2$ to superoxide ($10^{-3}$ $M^{-1}$ $s^{-1}$),[34] and equivalent to $O_2$ consumption by purified PSI (~$10^5$ $M^{-1}$ $s^{-1}$).[35] Thus, the ORR kinetics of Flv1 and Flv3 are consistent with the proposed function in protecting PSI, and photosynthetic electron transport, from $O_2$ induced damage.[36, 37]

The observation of cooperative NAD(P)H binding in Flv1 and Flv3 is so far unique among $O_2$-reducing FDPs and is a direct result of incorporation of the NAD(P)H binding oxidoreductase domain. The $O_2$ detoxifying FDP from *Clostridium difficile* that incorporates a NADH:rubredoxin oxidoreductase domain also catalyzes NADH-dependent ORR, however a kinetic profile was not reported.[17] Cooperative binding of NAD(P)H by Flv homodimers probably results from long-range interactions between NAD(P)H binding sites of the individual subunits. Based on our observations that Flv1 and Flv3 have similar kinetic properties, we hypothesize that the ORR activity of a proposed Flv1/Flv3 heterodimer[36, 38] would most likely be an average of the Flv1 and Flv3 activity profiles, and thus similar to homodimers.

Considering that ROS is detrimental to the functionality of photosynthetic electron transport, it is significant that Flv1 and Flv3 operate by cooperative kinetics to efficiently catalyze ORR. Essentially Flv1 and Flv3 are in a low reactive state (are "switched off") when either $O_2$ or NAD(P)H levels are low, i.e. conditions where catalysis would be prone to incomplete reduction of $O_2$ and more prone to generate ROS. On the other hand, small increases in both NAD(P)H and $O_2$ levels (~2-fold) lead to dramatic increases in ORR reaction rates to facilitate fast

$O_2$ consumption. By operating in this kinetic regime, Flvs efficiently catalyze ORR while minimizing formation of ROS under highly variable $O_2$ levels and reductant availability conditions that might arise, for example, during photosynthesis under natural fluctuations of light and metabolic rates of $CO_2$ fixation.

## Conflicts of interest

There are no conflicts to declare.

## Acknowledgements

This work was authored in part by Alliance for Sustainable Energy, LLC, the manager and operator of the National Renewable Energy Laboratory for the U.S. Department of Energy (DOE) under Contract No. DE-AC36-08GO28308. Funding was provided by the U.S. Department of Energy Office of Basic Energy Sciences, Division of Chemical Sciences, Geosciences, and Biosciences, Photosynthetic Systems Program. The U.S. Government and the publisher, by accepting the article for publication, acknowledges that the U.S. Government retains a nonexclusive, paid-up, irrevocable, worldwide license to publish or reproduce the published form of this work, or allow others to do so, for U.S. Government purposes. The Mass Spectrometry Facility at MSU is supported in part by the Murdock Charitable Trust and an NIH IDEA program grant P20GM103474. The authors would like to thank the Montana State University Microfabrication Facility for help in the preparation of gold-coated borosilica capillaries for non-covalent mass spectrometry.

## Experimental

#### Protein expression and purification

Flv1 and Flv3 were each codon optimized with the addition of a N-terminal StrepII-tag and cloned into pCDFDuet. Expressions were performed in *E. coli* BL21 (DE3) Rosetta-2 as follows. 5 mL of Terrific Broth (TB) media (EMD Millipore) supplemented with Streptomycin 50 μg $mL^{-1}$ was inoculated with freshly transformed cells and cultured overnight at 37 °C, 250 rpm. Cells were harvested at 4,000 rpm, 5 min, washed, resuspended in fresh TB and used to inoculate 50 mL of TB plus Streptomycin (1:50 dilution) cultured at 37 °C, 250 rpm to an OD600 = 0.6. The culture was diluted (1:100) into 1 L of TB plus Streptomycin, FMN (10 μM), and FAD (10 μM), and grown to an $OD_{600}$ = 0.4 at 37 °C. Ferric ammonium citrate was added to a final concentration of 2 mM and cultures were grown another 30 min. For induction, 1.5 mM IPTG was added and cultures were grown overnight at 37 °C. Cells were collected at 5000 rpm, washed with buffer A (50 mM Tris-HCl, 200 mM NaCl, 5% glycerol, pH 8.3), and frozen at -80 °C.

Cells were lysed (Microfluidics) following addition of a protease inhibitor (Roche), lysozyme, and 12 μL benzonase (30 units, Pierce). A cell-free lysate was prepared by high-speed centrifugation (45,000 rpm, 1 h, 4 °C), and the soluble fraction was applied to Strep XT resin (200 mM Tris-HCl pH 8.3, 200 mM NaCl, 5% glycerol). Flv containing fractions were collected based on A280. The purified Flvs were exchanged to 50 mM MOPS, 5% glycerol, pH 7 and stored at 4 °C. Protein concentrations were estimated using the Bradford assay with BSA as the standard. Purity was assessed by SDS-PAGE. Purified Flvs were incubated overnight with a 10-fold molar excess of FMN, FAD and ferrous ammonium sulfate. Excess flavins and ferrous ammonium sulfate were removed by spin dialysis using 10 kDa molecular weight cut off filters.

Fe content (1 mL samples, 3-4 μM) was determined using the method by Fish.[39] Fe standards were prepared by dilution of a commercial Fe AA standard (Ricca Chemical Co.). Flavin content (1 mL samples, 3-4 μM) and type were determined as previously described.[23] The flavin content of Flvs was determined as previously described.[23] Briefly, samples were heated to 100 °C and centrifuged to precipitate the protein fraction. An aliquot of the supernatant was treated with 10 mU of phosphodiesterase (PDE, Sigma) to convert the FAD to FMN. The ratio of FAD:FMN was calculated from the change in sample fluorescence before and after treatment using the equation:

$$\frac{\mathrm{FAD}}{\mathrm{FMN}} = \frac{10 * \frac{F_{PDE}}{F_0} - 10)}{(10 - \frac{F_{PDE}}{F_0})}$$

Where $F_0$ is the sample fluorescence after precipitation and $F_{PDE}$ is the sample fluorescence after PDE treatment.

#### Flv NAD(P)H oxidation kinetics

The change in NAD(P)H concentration over time was measured by UV-Vis spectroscopy (Cary). Solutions were prepared from a stock of 1 mM NAD(P)H diluted in air saturated 50 mM MOPS, 5% glycerol, pH 7 (223 μM $O_2$ at an altitude of 1730 m), and concentrations verified by $A_{340}$ ($\varepsilon_{340nm}$ = 6220 $M^{-1}$ $cm^{-1}$). After addition of Flv (2.5 nM final concentration) the change in NAD(P)H concentration was measured with stirring for 2 min, and the $A_{340}$ value collected every 0.0083 s. $O_2$ saturated (1066 μM) reactions were performed with 320 μM NAD(P)H and 10 nM Flv in a sealed cuvette. Rate results were fit to the steady-state Hill equation;

(1) $v = V_{\max}\left(\frac{[S]^n}{K' + [S]^n}\right)$

and steady-state Michaelis-Menten equation;

(2) $v = V_{\max}\left(\frac{[S]}{K' + [S]}\right)$.

#### Flv ORR kinetics

Membrane Inlet Mass Spectrometry (Hiden) was used to measure $O_2$ levels in 3 ml ORR reactions consisting of Flv (12.5 μM final concentration), 1 mM NAD(P)H in 50 mM MOPS, 5%

glycerol, pH 7 buffer. $O_2$ concentrations were 35, 107, 142, 223.3, 335, 448, 778, and 1066 μM. The $O_2$ levels of reactions were prepared in the absence of Flv, reactions at <223 μM were prepared by sparging with Ar and addition of $O_2$ saturated buffer, reactions at >223 μM were prepared by sparging with 100% $O_2$ and addition of air saturated buffer (223 μM). Each reaction was equilibrated for 20-30 min and the baseline $O_2$ voltage level was recorded to generate a calibration curve for $O_2$ concentration versus voltage. The Ar sparged Flv solutions (final concentration 12.5 μM) were added and the change in in dissolved $O_2$ was monitored over time. Rate results were fitted to steady-state Hill (Eqn 1) and Michaelis-Menten (Eqn 2) equations.

**NAD(P)H equilibrium binding kinetics**

Fluorescence binding titrations were measured in anaerobic samples of Flv. Samples contained 200 nM Flv in 50 mM MOPS, 5% glycerol, pH 7. Reduced pyridine nucleotides were added in an anaerobic glove box ($N_2$ atmosphere) and sealed. Fluorescence spectra were collected using an excitation wavelength of 285 nm and an emission window 300 – 500 nm, with both slit widths set at 8 nm (Fluorolog 3, Horiba). The binding isotherm was calculated using the intrinsic protein fluorescence emission signal at 348 nm with a correction factor for the inner filter effect as previously described.[60] To fit the equilibrium binding isotherm, we used the following equations (Eqns 3-7):

(3) $$\frac{\Delta F}{\Delta F_{\mathrm{MAX}}} = \frac{[\mathrm{Flv_{bound}}]}{[\mathrm{Flv_{total}}]}$$

(4) $$[\mathrm{Flv_{bound}}] = [\mathrm{NAD(P)H_{bound}}]$$

(5) $$[\mathrm{NAD(P)H_{free}}] = [\mathrm{NAD(P)H_{total}}] - [\mathrm{NAD(P)H_{bound}}]$$

Where:

(6) $$\Delta F = F_{\mathrm{NAD(P)H}} - F_0$$

$F_{\mathrm{NAD(P)H}}$ is the fluorescence at 348 nm a at given concentration of reduced pyridine nucleotide, and $F_0$ is the fluorescence at 348 nm for Flv alone. The dissociation constant ($K_d$) and the cooperativity (Hill) coefficient ($n$) were determined by fitting the data to the sigmoidal model equation:

(7) $$\Delta F = \frac{\Delta F_{\mathrm{MAX}}[\mathrm{NAD(P)H_{Free}}]^n}{K_d^{\mathrm{h}} + [\mathrm{NAD(P)H_{Free}}]^n}$$

**Oligomeric state of Flv3 and interactions within homodimers**

The oligomeric state of Flv3 was examined using chemical cross-linking as previously described.[40] Briefly, Flv3 samples at 10 μM concentration were chemically cross-linked with 1 mM bis(sulfosuccinimidyl)suberate (BS3) (Thermo-Fisher) in 50 mM HEPES, 150 mM NaCl buffer, pH 7.2 at room temperature for 15 and 30 min. Reactions were quenched with 120 mM Tris, pH 8. After 15 min incubation, resulting mixtures were separated on SDS-PAGE (4-20% linear gradient mini gel, Bio-Rad) and stained with Coomassie Brilliant Blue (Thermo-Fisher). Next, the major protein bands were subjected to overnight in-gel trypsin digestion according to the standard protocol recommended by the manufacturer using a trypsin (Promega) protease:complex ratio of 1:50. Proteins were identified as described[41] using a maXis Impact UHR-QTOF instrument (Bruker Daltonics) interfaced with a Dionex 3000 nano-uHPLC (Thermo-Fisher) followed by data analysis in SearchGUI/Peptide Shaker v.1.13.6.[42]

The cofactor composition identification was performed in denaturing conditions as previously described[43] using a Bruker Micro-TOF (Bruker Daltonics) coupled to a 1290 ultrahigh pressure (UPLC) series chromatography stack (Agilent Technologies). Because FMN was cleanly separated from Flv3 during the reverse-phase chromatography step, it's association with the protein is through a non-covalent interaction (Figure 3b).

Protein-cofactor interactions of Flv3 complex were investigated using native (non-covalent) mass spectrometry on a SYNAPT G2-Si instrument (Waters) as previously described.[44] Briefly, the Flv3 complex sample was buffer exchanged into 200 mM ammonium acetate, pH 7 (Sigma-Aldrich) using 3 kDa cutoff filters (Pall corporation) and infused from in-house prepared gold-coated borosilicate glass capillaries to the electrospray source at various protein concentrations of 1-5 μM and a flow rate around 90 nL $min^{-1}$. The instrument was tuned for high m/z range and operated in the following settings: source temperature 30 °C, capillary voltage 1.7 kV, trap bias voltage 16 V and argon flow in collision cell (trap) 7 mL $min^{-1}$. Transfer collision energy was held at 10 V while trap energy varied between 10-100 V. Data analysis was performed in MassLynx software version 4.1 (Waters). By carefully adjusting the energy applied during ion transmission it was possible to capture three distinct species: (i) a cofactor replete holo-homodimer (four flavins, four Fe atoms), (ii) a cofactor deficient apo-homodimer, and (iii) a partially dissociated intermediate homodimer with two flavins (Figures 3c and 3d).

Protein-protein interactions within the Flv3 homodimer were examined using surface labelling protocols.[45, 46] Briefly, Flv3 samples at 10 μM concentration were surface labelled in the presence of 50 mM 1-ethyl-3-(3-dimethylaminopropyl)carbodiimide (EDC, Thermo-Fisher) and 2 M glycine ethyl ester (GEE, Sigma-Aldrich) in 100 mM sodium phosphate buffer, pH 6 at room temperature. The reaction was quenched after three, five, and ten minutes by the addition of 1 μL of 1 M Tris-HCl, pH 8. In the second reaction, the Flv3 homodimers (10 μM) were surface labelled with 0.3 mM dansyl chloride (DnsCl, Acros) in 100 mM sodium phosphate buffer, pH 8 at room temperature. The reaction was quenched after 5, 10, and 15 min with the addition of 2 μL of 100 mM ammonium acetate, pH 8. Resulting mixtures from GEE and DnsCl labelling were separated on SDS-PAGE (4-20% linear gradient mini gel, Bio-Rad) and stained with Coomassie Brilliant Blue (Thermo-Fisher). Protein bands were processed and analyzed as described above. Identification of the labelled residues were

done in SearchGUI/Peptide Shaker v.1.13.6 with custom modifications for DnsCl (Unimod accession number 139; mass of 233.051 Da; reporter ions 171.104 Da and 235.051 Da on the side chain of lysine and/or serine residue) and GEE (mass of 86.0368 Da and 57.0215 Da on the side chain of glutamic and/or aspartic acid residue).

Protein homology models were generated by Phyre2[47] and energy-minimized models were docked using ClusPro2 with restrictions derived from labelling experiments.[48-50] Ligand binding site prediction was run in 3DLigandSite.[51] Molecular graphics were created using the UCSF Chimera package.[28] The twelve protein templates were selected to model Flv3 protein based on heuristics to maximize confidence, percentage identity and alignment coverage (PDB IDs: 1VME, 2Q9U[8], 1YCH[52], 4D02[53], 1E5D[11], 2OHI[54] and for the oxidoreductase domain: 5ZC2[55], 3RH7, 4HX6[56], 3K87[57], 3NFW[58]. The final models had 99% of residues modelled at the confidence higher than 90%. Binding sites were predicted by 3DLigandSite, based on 20 and 8 known protein structures containing diiron and FMN, respectively. By using a similar structural approach, the 3DLigandSite algorithm predicted association of the Flv protein oxidoreductase domain with FMN (18 templates: 3CB0, 2D36, 2D37, 2D38, 1I0S, 1USF, 1I0R, 1YOA, 3BNK, 1EJE, 1USC, 2D5M, 2R6V, 3HMZ, 2PTF, 3E4V, 2NR4, 2IML), FAD (6 templates: 3K88, 3K87, 1YOA, 1RZ1, 1RZ0, 2ED4) and NAD(P)H (7 templates: 3K88, 2D37, 1RZ1, 2ED4 and 2D38, 1I0S, 1USF).

#### UV-Vis and EPR spectroscopy of Flv3

Anaerobic UV-Vis titrations were performed on 25 µM Flv3 in 50 mM MOPS, 5% glycerol, pH 7 with a total volume of 2 ml. Samples were prepared under 100% $N_2$ in an anaerobic glove box. Addition of 100 mM sodium dithionite and NADH were added by gas tight syringe 1 µl at a time to achieve the desired molar ratios of reducing agent:Flv3. The total volume was changed by 0.5%. Spectra were collected on a Cary 4000 UV-Vis spectrophotometer.

Flv samples (80-100 µM enzyme concentration, 200 µL final volume) were prepared for EPR spectroscopy in the as-isolated state following purification and by addition of either NAD(P)H (5 mM final) or sodium dithionite (5 mM final) in 50 mM HEPES-NaOH, pH 7.5; 300 mM NaCl; 15% glycerol. Anaerobic samples were prepared by sparging under Ar gas for 60 min and then transferred to an anaerobic Mbraun box under 100% $N_2$ for treatment with either NADH or sodium dithionite. Low-temperature EPR spectra were recorded on a Bruker ELEXSYS E500 CW X- band spectrometer equipped with a SHQ Bruker resonator and in cavity cryogen-free VT system. Typical EPR parameters: microwave frequency, 9.38 GHz; microwave power, 1 mW; sample temperature, 5K; modulation amplitude, 10.0 G; modulation frequency, 100 kHz. For temperature dependence spectra series, sample temperature was varied from 5K to 80K. For power dependence spectra series, microwave power was varied from 0.001 to 200 mW. Spectra were processed with OriginPro and manually baseline corrected and background subtracted. Simulations of spectra were carried out using the EasySpin package.[59]

## Notes and references

1. J. B. Vicente, M. C. Justino, V. L. Gonçalves, L. M. Saraiva and M. Teixeira, *Methods Enzymol.*, 2008, **437**, 21-45.
2. Y. Helman, D. Tchernov, L. Reinhold, M. Shibata, T. Ogawa, R. Schwarz, I. Ohad and A. Kaplan, *Current Biology*, 2003, **13**, 230-235.
3. J. B. Vicente, C. M. Gomes, A. Wasserfallen and M. Teixeira, *Biochem. Biophys. Res. Commun.*, 2002, **294**, 82-87.
4. A. Alboresi, M. Storti and T. Morosinotto, *New Phytologist*, 2019, **221**, 105-109.
5. A. Kulkarni, S. Siahrostami, A. Patel and J. K. Nørskov, *Chem. Rev.*, 2018, **118**, 2302-2312.
6. M. L. Pegis, C. F. Wise, D. J. Martin and J. M. Mayer, *Chem. Rev.*, 2018, **118**, 2340-2391.
7. Y. Allahverdiyeva, J. Isojarvi, P. Zhang and E. M. Aro, *Life*, 2015, **5**, 716-743.
8. A. Di Matteo, F. M. Scandurra, F. Testa, E. Forte, P. Sarti, M. Brunori and A. Giuffrè, *J. Biol. Chem.*, 2008, **283**, 4061-4068.
9. C. Frazão, G. Silva, C. M. Gomes, P. Matias, R. Coelho, L. Sieker, S. Macedo, M. Y. Liu, S. Oliveira and M. Teixeira, *Nat. Struct. Mol. Biol*, 2000, **7**, 1041-1045.
10. J. B. Vicente, M. A. Carrondo, M. Teixeira and C. Frazao, *Methods Enzymol.*, 2008, **437**, 3-19.
11. C. Frazão, G. Silva, C. M. Gomes, P. Matias, R. Coelho, L. Sieker, S. Macedo, M. Y. Liu, S. Oliveira, M. Teixeira, A. V. Xavier, C. Rodrigues-Pousada, M. A. Carrondo and J. Le Gall, *Nat. Struct. Mol. Biol*, 2000, **7**, 1041-1045.
12. G. Shimakawa, K. Shaku, A. Nishi, R. Hayashi, H. Yamamoto, K. Sakamoto, A. Makino and C. Miyake, *Plant Physiol.*, 2015, **167**, 472-480.
13. P. T. Borges, C. V. Romão, L. M. Saraiva, V. L. Gonçalves, M. A. Carrondo, M. Teixeira and C. Frazão, *J. Struct. Biol.*, 2019, **205**, 91-102.
14. R. Silaghi-Dumitrescu, E. D. Coulter, A. Das, L. G. Ljungdahl, G. N. Jameson, B. H. Huynh and D. M. Kurtz, *Biochemistry*, 2003, **42**, 2806-2815.
15. R. E. Frederick, J. D. Caranto, C. A. Masitas, L. L. Gebhardt, C. E. MacGowan, R. J. Limberger and D. M. Kurtz Jr, *Journal of Biological Inorganic Chemistry*, 2015, **20**, 603-613.
16. S. Kihara, D. A. Hartzler and S. Savikhin, *Biophysical Journal*, 2014, **106**, 1882-1889.
17. F. Folgosa, M. C. Martins and M. Teixeira, *Sci. Rep*, 2018, **8**, 10164.
18. J. B. Vicente, F. Testa, D. Mastronicola, E. Forte, P. Sarti, M. Teixeira and A. Giuffrè, *Arch. Biochem. Biophys.*, 2009, **488**, 9-13.
19. J. W. LaMattina, M. Delrossi, K. G. Uy, N. D. Keul, D. B. Nix, A. R. Neelam and W. N. Lanzilotta, *Biochemistry*, 2017, **56**, 845-855.
20. J. E. Sanchez, P. G. Gross, R. W. Goetze, R. M. Walsh Jr, W. B. Peeples and Z. A. Wood, *Biochemistry*, 2015, **54**, 3360-3369.
21. M. Bouhaddou and M. R. Birtwistle, *Mol. Omics*, 2014, **10**, 1824-1832.
22. C. Tanford, J. A. Reynolds and E. A. Johnson, *Proc. Natl. Acad. Sci. USA*, 1985, **82**, 4688-4692.

23. A. Aliverti, B. Curti and M. A. Vanoni, in *Flavoprotein Protocols*, 1999, pp. 9-23.
24. J. B. Vicente and M. Teixeira, *J. Biol. Chem.*, 2005, **280**, 34599-34608.
25. J. B. Vicente, V. Tran, L. Pinto, M. Teixeira and U. Singh, *Eukaryot. Cell*, 2012, **11**, 1112-1118.
26. E. I. Solomon, T. C. Brunold, M. I. Davis, J. N. Kemsley, S.-K. Lee, N. Lehnert, F. Neese, A. J. Skulan, Y.-S. Yang and J. Zhou, *Chem. Rev.*, 2000, **100**, 235-350.
27. B. J. Wallar and J. D. Lipscomb, *Chem. Rev.*, 1996, **96**, 2625-2658.
28. E. F. Pettersen, T. D. Goddard, C. C. Huang, G. S. Couch, D. M. Greenblatt, E. C. Meng and T. E. Ferrin, *J. Comput. Chem.*, 2004, **25**, 1605-1612.
29. D. Yun, R. García-Serres, B. M. Chicalese, Y. H. An, B. H. Huynh and J. M. Bollinger, *Biochemistry*, 2007, **46**, 1925-1932.
30. M. J. Ryle, A. Liu, R. B. Muthukumaran, R. Y. N. Ho, K. D. Koehntop, J. McCracken, L. Que and R. P. Hausinger, *Biochemistry*, 2003, **42**, 1854-1862.
31. M. C. Martins, C. Romão, F. Folgosa, P. T. Borges, C. Frazão and M. Teixeira, *Free Radic. Biol. Med*, 2019, **in press**.
32. R. Silaghi-Dumitrescu, K. Y. Ng, R. Viswanathan and D. M. Kurtz, *Biochemistry*, 2005, **44**, 3572-3579.
33. M. Tamoi, T. Miyazaki, T. Fukamizo and S. Shigeoka, *Plant J.*, 2005, **42**, 504-513.
34. J. Golbeck and R. Radmer, in *Advances in photosynthesis research.(Ed. C Sybesma) pp*, 1984, vol. 1, pp. 561-561.564.
35. M. A. Kozuleva and B. N. Ivanov, *Plant Cell Physiol.*, 2016, **57**, 1397-1404.
36. Y. Allahverdiyeva, H. Mustila, M. Ermakova, L. Bersanini, P. Richaud, G. Ajlani, N. Battchikova, L. Cournac and E. M. Aro, *Proc Natl Acad Sci U S A*, 2013, **110**, 4111-4116.
37. Y. Allahverdiyeva, M. Suorsa, M. Tikkanen and E. M. Aro, *J Exp Bot*, 2015, **66**, 2427-2436.
38. H. Mustila, P. Paananen, N. Battchikova, A. Santana-Sánchez, D. Muth-Pawlak, M. Hagemann, E.-M. Aro and Y. Allahverdiyeva, *Plant Cell Physiol.*, 2016, pcw047.
39. W. W. Fish, in *Methods Enzymol.*, 1988, vol. 158, pp. 357-364.
40. R. N. Ledbetter, A. M. Garcia Costas, C. E. Lubner, D. W. Mulder, M. Tokmina-Lukaszewska, J. H. Artz, A. Patterson, T. S. Magnuson, Z. J. Jay and H. D. Duan, *Biochemistry*, 2017, **56**, 4177-4190.
41. Z.-Y. Yang, R. Ledbetter, S. Shaw, N. Pence, M. Tokmina-Lukaszewska, B. Eilers, Q. Guo, N. Pokhrel, V. L. Cash and D. R. Dean, *Biochemistry*, 2016, **55**, 3625-3635.
42. M. Vaudel, J. M. Burkhart, R. P. Zahedi, E. Oveland, F. S. Berven, A. Sickmann, L. Martens and H. Barsnes, *Nat. Biotechnol*, 2015, **33**, 22-24.
43. S. Poudel, M. Tokmina-Lukaszewska, D. R. Colman, M. Refai, G. J. Schut, P. W. King, P.-C. Maness, M. W. Adams, J. W. Peters and B. Bothner, *Biochim. Biophys. Acta*, 2016, **1860**, 1910-1921.
44. M. L. Luo, R. N. Jackson, S. R. Denny, M. Tokmina-Lukaszewska, K. R. Maksimchuk, W. Lin, B. Bothner, B. Wiedenheft and C. L. Beisel, *Nucleic Acids Res.*, 2016, **44**, 7385-7394.
45. H. Zhang, J. Wen, R. Y. Huang, R. E. Blankenship and M. L. Gross, *Int. J. Mass Spectrom*, 2012, **312**, 78-86.
46. G. J. Schut, N. Mohamed-Raseek, M. Tokmina-Lukaszewska, D. W. Mulder, D. M. N. Nguyen, G. L. Lipscomb, J. P. Hoben, A. Patterson, C. E. Lubner, P. W. King, J. W. Peters, B. Bothner, A.-F. Miller and M. W. W. Adams, *J. Biol. Chem.*, 2019, **294**, 3271-3283.
47. L. A. Kelley, S. Mezulis, C. M. Yates, M. N. Wass and M. J. Sternberg, *Nat. Protoc*, 2015, **10**, 845-858.
48. S. R. Comeau, D. W. Gatchell, S. Vajda and C. J. Camacho, *Bioinformatics*, 2004, **20**, 45-50.
49. D. Kozakov, D. Beglov, T. Bohnuud, S. E. Mottarella, B. Xia, D. R. Hall and S. Vajda, *Proteins*, 2013, **81**, 2159-2166.
50. D. Kozakov, R. Brenke, S. R. Comeau and S. Vajda, *Proteins*, 2006, **65**, 392-406.
51. M. N. Wass, L. A. Kelley and M. J. Sternberg, *Nucleic Acids Res.*, 2010, **38**, W469-W473.
52. R. Silaghi-Dumitrescu, D. M. Kurtz, L. G. Ljungdahl and W. N. Lanzilotta, *Biochemistry*, 2005, **44**, 6492-6501.
53. C. V. Romão, J. B. Vicente, P. T. Borges, B. L. Victor, P. Lamosa, E. Silva, L. Pereira, T. M. Bandeiras, C. M. Soares, M. A. Carrondo, D. Turner, M. Teixeira and C. Frazão, *J. Mol. Biol.*, 2016, **428**, 4686-4707.
54. H. Seedorf, C. H. Hagemeier, S. Shima, R. K. Thauer, E. Warkentin and U. Ermler, *FEBS J.*, 2007, **274**, 1588-1599.
55. A. Yuenyao, N. Petchyam, N. Kamonsutthipaijit, P. Chaiyen and D. Pakotiprapha, *Arch. Biochem. Biophys.*, 2018, **653**, 24-38.
56. C.-Y. Chang, J. R. Lohman, H. Cao, K. Tan, J. D. Rudolf, M. Ma, W. Xu, C. A. Bingman, R. M. Yennamalli, L. Bigelow, G. Babnigg, X. Yan, A. Joachimiak, G. N. Phillips and B. Shen, *Biochemistry*, 2016, **55**, 5142-5154.
57. B. N. Webb, J. W. Ballinger, E. Kim, S. M. Belchik, K.-S. Lam, B. Youn, M. S. Nissen, L. Xun and C. Kang, *J. Biol. Chem.*, 2010, **285**, 2014-2027.
58. Y. Zhang, T. E. Edwards, D. W. Begley, A. Abramov, K. B. Thompkins, M. Ferrell, W. J. Guo, I. Phan, C. Olsen, A. Napuli, B. Sankaran, R. Stacy, W. C. Van Voorhis, L. J. Stewart and P. J. Myler, *Acta Cryst. F*, 2011, **67**, 1100-1105.
59. S. Stoll and A. Schweiger, *J. Magn. Reson.*, 2006, **178**, 42-55.
60. M. O. Palmier and S. R. Van Doren, *Anal. Biochem.*, 2007, **371**, 43-51.

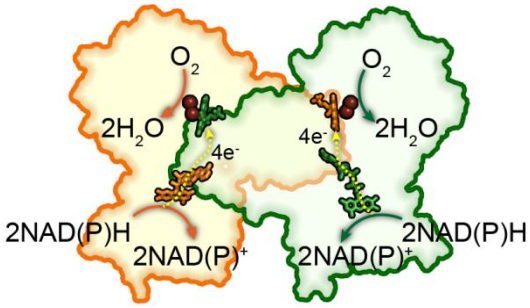


Flavodiirons catalyze oxygen reduction using non-heme iron sites (brown spheres) involving flavin (green, orange VDW) mediated electron transfer (yellow arrows).